Available online at www.sciencedirect.com
ScienceDirect
Journal of Power Sources 166 (2007) 64–67
JOURNAL OF POWER SOURCES
www.elsevier.com/locate/jpowsour

Short communication

Nucleation of nanometer-scale electrocatalyst particles in solid oxide fuel cell anodes

B.D. Madsen, W. Kobsiriphat, Y. Wang, L.D. Marks, S.A. Barnett *

Northwestern University, Materials Science and Engineering Department, 2220 Campus Drive, Evanston, IL 60208, USA

Received 18 December 2006; accepted 29 December 2006
Available online 16 January 2007

Abstract

This letter describes a method for forming Ru nanoclusters on oxide anode surfaces during the initial stages of solid oxide fuel cell operation, yielding improved anode performance without additional processing steps. Transmission electron microscope and X-ray photoelectron spectroscopy observations showed that Ru nanoclusters precipitated onto $La_{0.8}Sr_{0.2}Cr_{0.82}Ru_{0.18}O_{3-\delta}$ surfaces after exposure to hydrogen at 800 °C, with Ru cluster size stabilizing at ≤5 nm for the longest times tested, ∼300 h. Solid oxide fuel cell tests were done in humidified hydrogen at 800 °C with $La_{0.8}Sr_{0.2}Cr_{0.82}Ru_{0.18}O_{3-\delta}$–GDC (GDC = Gd-doped ceria) anodes on LSGM electrolyte-supported cells. Cell power density increased over the first ∼50 h of cell operation from ∼200 to 400 mW cm^{-2} due to an anode polarization resistance decrease from ∼0.6 to <0.2 Ω cm^2.
© 2007 Elsevier B.V. All rights reserved.

Keywords: Solid oxide fuel cell; Nanoparticle; Catalyst; Ruthenium; Lanthanum chromite

1. Introduction

There has been considerable interest in incorporating nanometer-scale structures into SOFCs to yield improved electrolyte and electrode performance. Nanoelectrolyte materials can provide increases in ionic conductivity by a factor of 10 or greater [1,2]. Similarly, decreasing electrode feature sizes into the nanometer range is expected to improve performance by increasing surface areas [3] and triple-phase boundary lengths [4]. While nanoscale materials can be stable at SOFC operating temperatures that are typically ≤800 °C [5], and may be as low as 500 °C [6], they typically coarsen into larger particles at the relatively high firing temperatures (up to 1400 °C) used to process SOFCs. One example of this is in the area of ceramic-based anodes [7], materials that are interesting because of their potential to work with hydrocarbon fuels [8], their good stability during redox cycling [8], and reduced sensitivity to sulfur-containing fuel impurities [9,10]. Electrochemical characteristics of ceramic anodes can be improved by adding a small amount of electrocatalyst nanoparticles [11], e.g. ≈5% Ni in $La_{0.8}Sr_{0.2}Cr_{0.98}V_{0.02}O_{3-\delta}$–$Ce_{0.9}Gd_{0.1}O_{1.95}$–Ni (LSCrV–GDC–Ni) anodes [12,13]. However, increasing the anode firing temperature to ≥1300 °C decreased SOFC power densities, a change attributed to coarsening of the Ni catalyst particles and the other anode phases [12].

Here we show a method for forming electrocatalytic nanoparticles on lanthanum chromite anode surfaces after the high-temperature firing and without additional processing steps. Ru was used since it is less susceptible than Ni to sintering and coking [14]. Instead of adding the Ru as a separate phase, it was dissolved in the lanthanum chromite phase. The Ru nanoparticles precipitated from the lanthanum chromite phase upon heating in hydrogen at the start of SOFC operation, accompanied by a dramatic reduction in anode polarization resistance.

2. Experimental procedures

Powders of $La_{0.8}Sr_{0.2}Cr_{0.82}Ru_{0.18}O_{3-\delta}$ (LSCrRu) and $La_{0.8}Sr_{0.2}CrO_{3-\delta}$ (LSCr) were synthesized by solid-state reaction at 1200 °C for 3 h, yielding particle sizes of ∼1–2 μm. All powders had X-ray diffraction (XRD) patterns similar to $La_{0.8}Sr_{0.2}CrO_{3-\delta}$, and no RuO_2 was detected in LSCrRu. SOFCs were made with anodes composed of 50 wt.% $(La_{0.8}Sr_{0.2})(Cr_{0.82}Ru_{0.18})O_{3-\delta}$ (LSCrRu) and 50 wt.% GDC. A few SOFCs with Ru-free anodes, LSCr–GDC, were prepared and tested for comparison.

* Corresponding author. Tel.: +1 847 491 2447; fax: +1 847 491 7820.
E-mail address: s-barnett@northwestern.edu (S.A. Barnett).

0378-7753/$ – see front matter © 2007 Elsevier B.V. All rights reserved.
doi:10.1016/j.jpowsour.2006.12.080

All SOFCs utilized $La_{0.9}Sr_{0.1}Ga_{0.8}Mg_{0.2}O_{3-\delta}$ (LSGM) electrolytes, ~400 μm thick, fabricated via solid-state reaction at 1250 °C followed by uniaxial pressing and sintering for 6 h at 1450 °C. The cathodes were $La_{0.6}Sr_{0.4}Co_{0.2}Fe_{0.8}O_{3-\delta}$ (LSCF)–GDC. The anodes and cathodes (0.5 cm^2 active area, ~50 μm thick) were screen printed on the LSGM electrolytes and fired for 3 h at 1200 and 1000 °C, respectively. Note that a La-doped ceria barrier layer is normally needed between Ni-YSZ anodes and LSGM electrolytes to prevent Ni-LSGM reactions and possible La out-diffusion from the LSGM electrolyte [15]; no barrier layers were needed with the present LSCrRu anodes. Au current collector grids were screen printed over the electrodes and contacted using Ag wires. Single cell tests were performed as described previously [8] using a four-wire setup for current–voltage and impedance spectroscopy (IS, BAS-Zahner IM-6) measurements. In life tests, the cells were first stabilized at temperature with Ar at the anode before starting humidified H_2 flow; times given are after the start of H_2 flow. Measurements on stable SOFCs (not presented here) indicated that the Ar was almost entirely purged from the anode compartment before the first electrical measurements (15 min).

3. Experimental results

Fig. 1 shows the electrical performance versus time after the onset of testing in humidified H_2 at 800 °C, for a typical SOFC with an LSCrRu–GDC anode. The maximum power density within the first ≈15 min of testing was ≈250 mW cm^{-2}, and increased continuously with time before stabilizing at 390 mW cm^{-2} at 100 h. Similar results were observed at other test temperatures, e.g. at 750 °C the power increased from 120 mW cm^{-2} (15 min) to 300 mW cm^{-2} (100 h).

Fig. 2 shows the voltage versus time at a current density of 0.6 A cm^{-2}—the cell was maintained at this condition over most of the 300 h test. The voltage increased rapidly during the first few hours of testing, with a slower increase over the next ~50 h, consistent with the result shown in Fig. 1. After ~100 h, the voltage was reasonably stable, decreasing by ≈2% over the next 200 h. The inset in Fig. 2 shows electrochemical impedance spectra taken at 15 min and 96 h at a cell voltage of 0.5 V. High frequency intercepts were at ≈0.4 Ω cm^2, and attributed to the ohmic resistance associated with the 0.4 mm thick LSGM electrolyte (conductivity ≈0.1 S cm^{-1} at 800 °C [16]). The low frequency arc, initially ≈0.6 Ω cm^2, decreased rapidly before stabilizing at ≈0.2 Ω cm^2, indicating that the power density increase with time was an electrode effect. Based on separate measurements of the LSCF–GDC cathodes yielding a relatively small polarization resistance of ~0.05 Ω cm^2 [12], the electrode resistance was primarily due to the anode. SOFCs identical to the above, but with LSCr–GDC anodes instead of LSCrRu–GDC, were also tested at 800 °C; maximum power density was lower, ≤240 mW cm^{-2}, and the minimum polarization resistance (at 0.5 V) higher, ≥1.6 Ω cm^2. This shows that the Ru substantially improved anode performance.

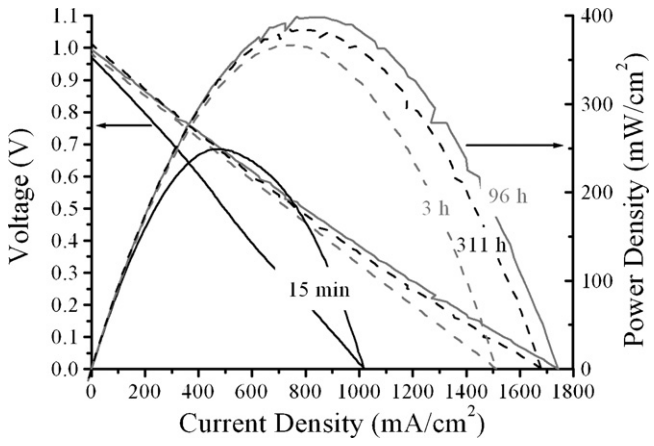

Fig. 1. Voltage and power density vs. current density at 800 °C, measured at various times after the start of humidified H_2 flow, for a typical cell with an LSCrRu–GDC anode.

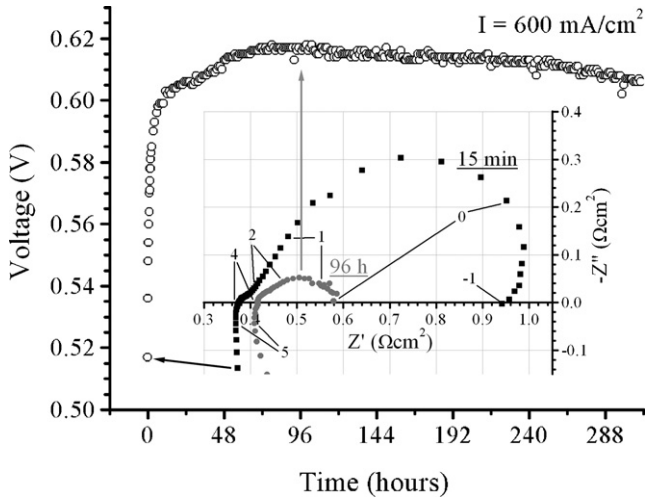

Fig. 2. Cell voltage vs. time for an SOFC operated at 0.6 A cm^{-2} in humidified H_2 at 800 °C. The inset shows electrochemical impedance spectra at 0.5 V taken after 15 min and 96 h, with arrows indicating the corresponding data in the voltage plot. Frequencies (10^x) for the impedance data are denoted for several data points. Note that the unusual shape of the 15 min arc at <1 Hz was presumably due to anode resistance changes during the EIS measurement (≈1 min/data point at lowest frequency).

LSCrRu powders were examined by transmission electron microscopy (TEM) before reduction and after a 45 h exposure to H_2 at 800 °C, i.e. SOFC anode conditions. The un-reduced LSCrRu powder, corresponding to the SOFC anode prior to testing, showed no unusual features. After reduction, nanoclusters were readily apparent on the surfaces of LSCrRu particles in scanning TEM (Fig. 3a) and high-resolution electron microscope (Fig. 3b) images. Nanocluster lattice fringes (see Fig. 3b) yielded atomic spacings in the (1 1 0) and (0 0 2) directions of 1.35 and 2.14 Å, respectively, that agree within 1% with reported values for hexagonal Ru [JCPDS card #70-0274]. Finally, note that LSCr (no Ru) powder was examined by TEM after 45 h reduction in H_2, and showed no nanoclusters.

X-ray photoelectron spectroscopy (XPS) analysis of LSCrRu showed a decrease of 1–2 eV in the Ru 3d peak positions after annealing in H_2 for 45 h (Fig. 4), to the energies expected for metallic Ru. The peak shifts indicate a reduction in the oxidation

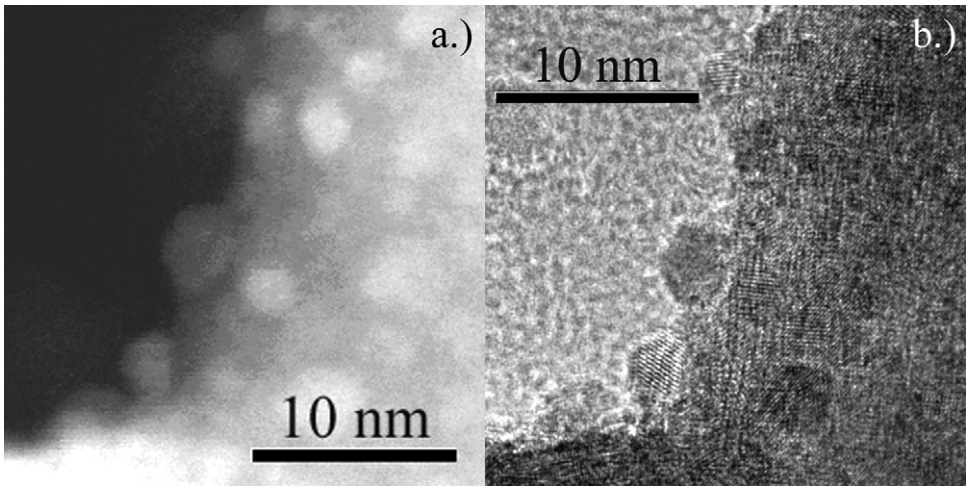

Fig. 3. $La_{0.8}Sr_{0.2}Cr_{0.82}Ru_{0.18}O_{3-\delta}$ after 45 h reduction in H_2 showing nanoparticles on the surface as observed by: (a) STEM and (b) HREM. Lattice fringes of the nanoparticles seen in (b) yield atomic spacings of 1.35 and 2.14 Å in the (1 1 0) and (0 0 2) directions, respectively, which agree with reported values for hexagonal Ru.

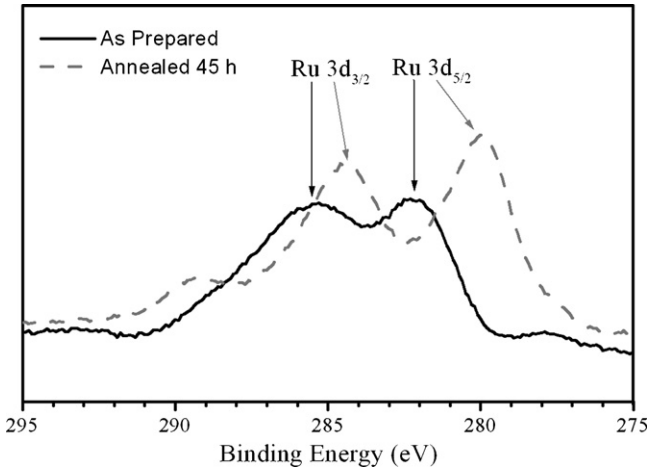

Fig. 4. X-ray photoelectron spectra comparing as-prepared $La_{0.8}Sr_{0.2}Cr_{0.82}Ru_{0.18}O_{3-\delta}$ and the same material after annealing for 45 h in H_2 at 800 °C. The peak positions after reduction are consistent with metallic Ru.

state of Ru located near the LSCrRu surface. These results show that Ru nanoparticles form on LSCrRu surfaces upon exposure to H_2 at elevated temperatures.

4. Discussion

Metal nanoparticle precipitation on oxide surfaces has been reported previously and shown to improve catalytic properties for automotive emissions control [17]. The novel features of the present results are the observation of nanoparticles on SOFC anodes, and their strong effect on electrochemical performance.

In order to form the nanoclusters, Ru presumably diffuses from within the LSCrRu particle to the surface. The amount of surface Ru at 45 h, estimated from the size (hemispherical with ≈5 nm diameter) and density ($\sim 4 \times 10^{12}$ cm^{-2}) of nanoclusters in Fig. 3, corresponded to ∼15% of the bulk Ru in an assumed 1000-nm-diameter spherical $La_{0.8}Sr_{0.2}Cr_{0.82}Ru_{0.18}O_{3-\delta}$ particle. Based on this rate of Ru accumulation, a minimum Ru diffusion coefficient D was estimated assuming for the moment that the Ru transport to the surface was limited by diffusion. A diffusion length L was estimated by noting that 15% of the Ru in a 1000-nm-diameter LSCrRu sphere is contained in a surface layer $L \sim 25$ nm thick. Taking a diffusion time $t = 45$ h, an approximate diffusion coefficient $D \sim L^2/t \sim 10^{-21}$ m^2 s^{-1} is obtained. This value is consistent with reported cation bulk diffusion coefficients in lanthanum chromite extrapolated to 800 °C [18].

Alternatively, Ru segregation may be limited by the single-phase field of LSCrRu. That is, removing too much Ru from LSCrRu may be thermodynamically unfavorable because it yields a highly non-stoichiometric (La and Sr rich) oxide [19]. This idea is supported by the fact that there was no evidence of La- or Sr-containing phases in the TEM or XRD data after reduction, as might be expected if most of the Ru segregated out of $La_{0.8}Sr_{0.2}Cr_{0.82}Ru_{0.18}O_{3-\delta}$.

The present results can be compared with similar $La_{1-x}Sr_xCr_{1-y}Ru_yO_{3-\delta}$ anode compositions that contained a yttria-stabilized zirconia second phase [14,20]. The best anode area-specific resistance, 3.7 Ω cm^2 at 750 °C in H_2–H_2O, was substantially worse than the present anodes, 0.45 Ω cm^2 at 750 °C, and no evidence of metallic Ru formation was reported. The present anodes showed area-specific resistances in hydrogen of 0.2 Ω cm^2 at 800 °C, comparable to the best reported ceramic anodes: 0.1–0.25 Ω cm^2 for $Sr_2Mg_{1-x}Mn_xMoO_{6-\delta}$ ($x = 0$–1) at 800 °C [21], 0.25 Ω cm^2 for $La_{0.75}Sr_{0.25}Cr_{0.5}Mn_{0.5}O_3$ anodes at 925 °C (with a $Ce_{0.8}Gd_{0.2}O_{2-\delta}$ interlayer) [22], and 0.2 Ω cm^2 for cerium-modified (La,Sr)(Ti,Ce)O_3 anodes at 850 °C [23]. It is possible that the present strategy, i.e. substituting a small amount of a suitable catalyst element for one of the cations in an oxide, could be employed to further improve on these or other anode oxides. The key requirements are that a suitable catalyst element is soluble in the oxide at high oxygen partial pressure (in air), and that the catalyst has a relatively low free energy of oxide formation (e.g. 120 kJ mol^{-1} for Ru at 800 °C [24]) such that a separate metallic phase precipitates out upon reduction.

Finally, two practical issues regarding these anodes, cost and long-term stability, should be discussed. Materials cost is not expected to be a problem for the present LSCrRu–GDC anodes. For an ~20 μm thick anode active layer, the Ru loading is only 0.4 mg cm^{-2}. Given a current market price of \$5.50 g^{-1} for Ru [25], and an SOFC power density of 0.4 W cm^{-2}, the Ru contributes only ≈\$5 kW^{-1} to the cost of the SOFC. Regarding stability, only slight degradation of SOFC performance was observed in the life test (Fig. 2). Also, initial TEM results showed no evidence of Ru nanocluster coarsening over 300 h. While these results are promising, more work on longer-term stability will clearly be needed. Note that in prior catalyst work, it was shown that precipitated nanoclusters were regenerated by oxidizing the reduced material, causing the catalyst metal to redissolve in the oxide, and then reducing, causing fresh metal nanoclusters to precipitate [17]; similar regeneration may be possible in SOFC anodes.

Acknowledgements

The authors acknowledge impedance spectroscopy measurements by Yuanbo Lin on LSCF–GDC cathodes on LSGM. This material is based upon work supported by the Department of Energy under Award Number DE-FG02-05ER46255.

References

[1] J.H. Hwang, T.O. Mason, Z. Phys. Chem. 207 (1/2) (1998) 21–38.
[2] I. Kosacki, C.M. Rouleau, P.F. Becher, J. Bentley, D.H. Lowndes, Solid State Ionics 176 (13/14) (2005) 1319–1326.
[3] S.B. Adler, J.A. Lane, B.C.H. Steele, J. Electrochem. Soc. 143 (11) (1996) 3554–3564.
[4] J.R. Wilson, W. Kobsiriphat, R. Mendoza, H.-Y. Chen, J.M. Hiller, D.J. Miller, K. Thornton, P.W. Voorhees, S.B. Adler, S.A. Barnett, Nat. Mater. 5 (7) (2006) 541–544.
[5] A.J. McEvoy, Solid State Ionics 132 (3/4) (2000) 159–165.
[6] Z. Zhan, Z. Shao, S.M. Haile, J. Ahn, P.D. Ronney, S.A. Barnett, Nature 435 (2005) 795–798.
[7] A. Atkinson, S.A. Barnett, R.J. Gorte, J.T.S. Irvine, A.J. McEvoy, M. Mogenson, S.C. Singhal, J. Vohs, Nat. Mater. 3 (2004) 17–27.
[8] B.D. Madsen, S.A. Barnett, Solid State Ionics 176 (2005) 2545–2553.
[9] R. Mukundan, E.L. Brosha, F.H. Garzon, Electrochem. Solid State Lett. 7 (1) (2004) A5–A7.
[10] L. Aguilar, S. Zha, S. Li, J. Winnick, M. Liu, Electrochem. Solid State Lett. 7 (10) (2004) A324–A326.
[11] J. Liu, B.D. Madsen, Z.Q. Ji, S.A. Barnett, Electrochem. Solid State Lett. 5 (6) (2002) A122–A124.
[12] B.D. Madsen, S.A. Barnett, accepted by J. Electrochem. Soc. (2006).
[13] B.D. Madsen, S.A. Barnett, in: S.C. Singhal, J. Mizusaki (Eds.), Proceedings of the Ninth International Symposium on Solid Oxide Fuel Cells, Electrochemical Society, Pennington, NJ, 2005, pp. 1185–1194.
[14] A.-L. Sauvet, J. Fouletier, F. Gaillard, M. Prime, J. Catal. 209 (2002) 25–34.
[15] Y. Lin, S.A. Barnett, Electrochem. Solid State Lett. 9 (6) (2006) A285–A288.
[16] K. Yamaji, Y. Xiong, T. Horita, N. Sakai, H. Yokokawa, in: S.C. Singhal (Ed.), Proceedings of the Seventh International Symposium on Solid Oxide Fuel Cells, Electrochemical Society, Pennington, NJ, 2001, pp. 413–421.
[17] H. Tanaka, M. Uenishi, M. Taniguchi, I. Tan, K. Narita, M. Kimura, K. Kaneko, Y. Nishihata, J.I. Mizuki, Catal. Today 117 (1–3) (2006) 321–328.
[18] N. Sakai, K. Yamaji, T. Horita, M. Ishikawa, H. Yokokawa, M. Dokiya, in: U. Stimming, S.C. Singhal, H. Tagawa, W. Lehnert (Eds.), Proceedings of the Fifth International Symposium on Solid Oxide Fuel Cells, Electrochemical Society, Pennington, NJ, 1997, pp. 1283–1290.
[19] S. Simner, J. Hardy, J. Stevenson, T. Armstrong, J. Mater. Sci. Lett. 19 (2000) 863–865.
[20] A.-L. Sauvet, J. Fouletier, Electrochim. Acta 47 (2001) 987–995.
[21] Y.-H. Huang, R.I. Dass, Z.-L. Xing, J.B. Goodenough, Science 312 (2006) 254–257.
[22] S. Tao, J.T.S. Irvine, J. Electrochem. Soc. 151 (2) (2004) A252–A259.
[23] O.A. Marina, L.R. Pederson, in: J. Huijismans (Ed.), Proceedings of the Fifth European Solid Oxide Fuel Cell Forum, European Fuel Cell Forum, 2002, pp. 481–489.
[24] K.T. Jacob, S. Mishra, Y. Waseda, J. Am. Ceram. Soc. 83 (7) (2000) 1745–1752.
[25] http://www.platinum.matthey.com.